Combining density functional theory (DFT) and collision cross-section (CCS) calculations to analyze the gas-phase behaviour of small molecules and their protonation site isomers

Jasper Boschmans[1], Sam Jacobs[2], Jonathan P. Williams[3], Martin Palmer[3], Keith Richardson[3], Kevin Giles[3], Cris Lapthorn[4], Wouter A. Herrebout[2], Filip Lemière[1], Frank Sobott[1,5,6]

[1]Biomolecular & Analytical Mass Spectrometry group, Department of Chemistry, University of Antwerp, Antwerp, Belgium, [2]Molecular Spectroscopy group, Department of Chemistry, University of Antwerp, Antwerp, Belgium, [3]Waters Corporation, Stamford Avenue, Wilmslow, SK9 4AX, UK, [4]Faculty of Engineering & Science, University of Greenwich, Medway Campus, Chatham, ME4 4TB, UK, [5]Astbury Centre for Structural Molecular Biology, University of Leeds, Leeds LS2 9JT, UK, [6]School of Molecular and Cellular Biology, University of Leeds, LS2 9JT, UK

1. Abstract

Electrospray ion mobility-mass spectrometry (IM-MS) data show that for some small molecules, two (or even more) ions with identical sum formula and mass, but distinct drift times are observed. In spite of showing their own unique and characteristic fragmentation spectra in MS/MS, no configurational or constitutional isomers are found to be present in solution. Instead the observation and separation of such ions appears to be inherent to their gas-phase behaviour during ion mobility experiments. The origin of multiple drift times is thought to be the result of protonation site isomers ('protomers'). Although some important properties of protomers have been highlighted by other studies, correlating the experimental collision cross-sections (CCS) with calculated values has proven to be a major difficulty. As a model, this study uses the pharmaceutical compound melphalan and a number of related molecules with alternative (gas-phase) protonation sites. Our study combines density functional theory (DFT) calculations with modified MobCal methods (e.g. nitrogen-based Trajectory Method algorithm) for the calculation of theoretical CCS

values. Calculated structures can be linked to experimentally observed signals, and a strong correlation is found between the difference of the calculated dipole moments of the protomer pairs and their experimental CCS separation.

2. Introduction

Ion mobility-mass spectrometry (IM-MS) is a separation and characterization technique that has proven to be applicable in many research fields since it started to gain popularity more than a decade ago with the introduction of the commercial Synapt system[1]. The drift time in ion mobility is determined by the collision cross-section (CCS) of an ion, which is a parameter related to its size, shape and charge. Originally used in structural studies investigating protein folding[2-9] and protein complexes[10-15], more and more researchers are starting to use commercial IM-MS instrumentation to investigate the separation, identification and gas-phase behaviour of small molecules. A possible application is the rapid separation of all types of isomers, based on their mobilities (drift times)[16-24]. Recently, a number of ion mobility studies have reported on the observation of protomers for aniline and the antibacterial agent norfloxacin[25-27]. These isobaric ions are gas-phase protonation site isomers, where the protons are located on different atoms. Although the position of a single H atom and the positive charge appear to have a very subtle effect on these small molecules, they can cause clear differences in drift times. Such differences can be relatively large for small molecules, and one would therefore typically expect that they are due to the presence of isomers or conformers (i.e. size and shape differences). In a recent study, Warnke *et al.* used IM-MS in combination with infrared multiple photon dissociation (IRMPD) spectroscopy to study the origin of benzocaine protomers[28]. Differences in N-H and O-H stretch vibrations showed that two alternative sites are protonated: the amine and, unexpectedly, also the carbonyl group. These data confirm that the large difference between the observed CCS values for this compound is caused by the different charge sites, rather than e.g. the consequence of a subsequent gas-phase rearrangement reaction. The appearance of alternative gas-phase protonation sites highlights the possibility of intra-molecular charge transfer during the electrospray process[28]. Anionic species show similar phenomena, as was recently reported by Galaverna *et al.* for benzoic acid de-protomers[29]. It also questions the localization of

charges in multiply protonated peptide and protein ions, important for computational structure and fragmentation prediction, which are frequently assumed to remain on basic, surface-exposed residues such as lysine and arginine during the ESI process.

Computational methods, such as molecular dynamics and quantum mechanical calculations, can support IM-MS observations (see Figure 1). These methods have become important tools for understanding and interpreting the experimental data, and they can potentially also be used to predict the separation of hypothetical charge isomers in ion mobility[30,31]. Interpretation of ion mobility data typically requires a conformational analysis of each protomer, after which all structures are optimized using DFT. This yields a set of geometries and associated partial atomic charges that can be used to compute the corresponding CCS values.

In this study we utilised the MobCal software[32], which provides three different algorithms; the Projection Approximation (PA), Exact Hard Sphere Scattering (EHSS) and the Trajectory Method (TM). Of these, the most widely used are the PA and TM. In both the PA and EHSS methods the molecule is represented as a collection of overlapping hard spheres. The CCS calculated by the PA is simply the rotational average of the projected area of this collection. While fast, the PA fails to model momentum transfer between the gas and analyte molecules as well as concave analyte structure and long range ion molecule interactions. In the EHSS method, a full hard sphere trajectory is calculated for each analyte-gas collision. This is a significantly more sophisticated model, and it has found utility as a fast method for calculating CCS of large molecular structures[33]. Long-range interactions, which are often significant for drug-like molecules, are necessarily ignored. The TM is the most sophisticated and computationally intensive of the commonly used methods. It involves a simulation of the trajectory of gas atoms through a superposition of Lennard-Jones potentials corresponding to the atoms in the analyte molecule. Polarisation of the gas molecules by the charge on the analyte molecule is also taken into account, but modifications to the original algorithm are required to adequately model interactions with polyatomic gases. More recently, the Projected Superposition Approximation (PSA) algorithm was introduced by Bleiholder *et. al*.[34-38] In this approach, which is used mainly for larger molecules, the PA cross section is modified to take into account the detailed three-dimensional structure of the analyte. Although previous studies of protomers made use of methods originally available in MobCal, they were not always able to accurately reproduce the experimental CCS

values[25,27]. It is believed that IM-MS separations using polyatomic drift gases (such as N_2 or CO_2) require a better representation of long-range interactions. The passage of a charged particle induces higher-order multipoles in the gas molecules, leading to additional (retarding) forces on the ion, and more collision geometries must be considered. Kim *et al.* proposed a modification to the existing trajectory method CCS calculation algorithms for N_2, which takes ion-quadrupole interactions and the orientation of non-spherical gas molecules into account[40,41]. This modification leads to significantly higher calculated CCS values, which better conform to the experimentally determined data. Only a few studies have used this new approach so far to correctly reproduce experimental CCS values[28,30,31,40-42]. Apart from protomer-related studies, Lavanant *et al.* used the modified algorithm to calculate CCS values for phosphoric acid clusters, which can be used for negative ion mode IM calibrations[43].

The present study investigates 1. the experimental separation of hypothetical protomers for 7 related compounds which share an amino and carbonyl function (in aniline, a benzene ring) as alternative protonation sites; 2. the effect of using different levels of theory for optimization of molecular geometry and charge distribution, 3. the ability to obtain theoretical CCS that closely match experimental values; 4. the importance of the analyte charge distribution itself (and the resulting dipole moment) in contrast to possible charge-driven changes in molecular structure, and 5. the ability to predict protomer separation in ion mobility experiments based on the difference in the calculated molecular dipole moments for hypothetical protomer pairs. This study tests the hypothesis that experimentally found protomers can be predicted reasonably well by differences in the calculated dipole moments. The results reported here inform choices of computational approaches for the prediction of protomer separation in ion mobility so that spectral interpretation software (e.g. in metabolomics) could be trained to detect such phenomena.

3. Results and discussion

3.1 IM-MS separation of protonation site isomers

Two distinct peaks are observed in the arrival time distribution (ATD) of melphalan (*m/z* 305) using nitrogen as drift gas: **I'** and **I"** (see Figure 2), which are centred around 169.9

137 Å^2 and 179.1 Å^2. However, for two other, closely related compounds,
138 dimethoxymelphalan ($DOCH_3$; **II**) and dihydroxymelphalan (DOH; **III**), we observe only
139 single and unique peaks (Figure 2), at 172.2 Å^2 for $DOCH_3$ and 165.3 Å^2 for DOH. We
140 also used CO_2 to perform ion mobility separations of $DOCH_3$ and DOH, but again only
141 single peaks were observed (data not shown).
142 Similar observations to those with melphalan were made for the local anaesthetic
143 *para*-benzocaine, an ethyl ester derivative of *para*-aminobenzoic acid (Figure 3). Two
144 peaks were found (**IV'** and **IV"**) at 131.7 Å^2 and 147.5 Å^2. For comparison, positional
145 isomers of benzocaine were also studied (Figure 3): ethyl 2-aminobenzoate
146 ("*ortho*-benzocaine") and ethyl 3-aminobenzoate ("*meta*-benzocaine"). The selected-ion
147 ATD of *ortho*-benzocaine shows only one peak at 135.2 Å^2 (**V**). For *meta*-benzocaine, two
148 peaks are observed (**VI'** and **VI"**) which correspond to CCS values of 133.6 Å^2 and 146.4
149 Å^2. For aniline, which we included here as a reference compound, we find two peaks as
150 reported previously[25] (**VII'** and **VII"**; see Figure 3), with CCS values of 112.9 Å^2 and 118.9
151 Å^2. Table 1 summarizes all experimental CCS values.
152
153 3.2 Calculating CCS values of melphalan protomers
154 Three possible protomers of melphalan were taken into account here: protonation at the
155 nitrogen atom of the NH_2 group (N_{AA}), the carboxyl group (O_{CO}) on the amino acid side,
156 and the nitrogen atom adjacent to the phenyl ring on the chloroethyl side (N_{Cl}). Based on
157 the solution basicity (i.e. pK_a) of the various functional groups in melphalan[44], O_{CO} and N_{Cl}
158 protonation seem less plausible (see Figure 2). Nonetheless, other protomer studies
159 have reported on oxygen-rich functional groups or even aromatic rings[25-28] as preferred
160 protonation sites. After performing a conformational analysis of melphalan and
161 subsequent DFT optimisation at the B3LYP/6-31G(d,p) level (hereafter referred to as
162 "standard" level), the CCS values for the optimised structures were calculated using a
163 modified version of MobCal where the TM code optimized for use with nitrogen (see
164 Figure 1). Table 2 gives an overview of the top 5 lowest-energy conformers of each
165 melphalan protomer, together with energies, overall Boltzmann weights, dipole moments
166 and calculated CCS values. Figure 4 visualizes the conformation and molecular
167 electrostatic potential (MEP) of each lowest-energy melphalan protomer.
168 From the three protomers considered here, the N_{AA} and N_{Cl} forms best match the
169 experimentally determined CCS_{N2}. This would indicate that the O_{CO} protomer is not
170 observed during the ion mobility experiments. The ΔCCS_{N2} between the calculated N_{AA}

and N_{Cl} protomers is 9.0 Å^2, which is a good match with the experimentally determined value of 9.2 Å^2.

3.3 Melphalan-related compounds: dihydroxymelphalan and dimethoxymelphalan

The study of melphalan derivatives, which unlike melphalan itself show only one observed drift time, allows us to investigate the factors that govern formation and separation of melphalan protomers more closely. A conformational analysis was performed for possible protomers of these compounds, and the resulting structures were optimised at "standard" level. Although DOH and $DOCH_3$ are chemically less complex structures than melphalan itself (i.e. no halogen atoms), the additional rotational flexibility yields more conformers and thus entails an added computational cost. For each lowest-energy protomer, the values are reported in Table 3 and structures are given in Figure 2. Calculated CCS values were also compared to the experimentally derived ones (172.2 Å^2 for $DOCH_3$ and 165.3 Å^2 for DOH). This allows us to evaluate the nitrogen-modified MobCal code, but could also show whether significantly different CCS values are calculated for protomers in cases where they are not experimentally resolved. The N_{AA} protomer for DOH has a considerably smaller calculated CCS (156.1 Å^2) than the experimentally observed value. The CCS of the N_{OH} protomer on the other hand (164.6 Å^2) is a close match with the experiment. For $DOCH_3$, the calculated CCS values of both hypothetical protomers (181.3 Å^2 and 182.3 Å^2) over-estimate the experimental CCS of 172.2 Å^2.

3.4 Other related small molecules: benzocaine isomers and aniline

Our calculation strategy was further evaluated against experimentally determined CCS values of benzocaine isomers and aniline (Table 4). For *para*-benzocaine, protonation of the carbonyl group gives a CCS_{N2} of 132.0 Å^2 for the lowest-energy structure after standard-level optimization, while the equivalent procedure for the amine-protonated species results in a CCS_{N2} value of 140.9 Å^2, which is significantly smaller than the experimental value (147.5 Å^2). While the theory correctly predicts the separation of the two protomers, it remains unclear why the calculated value for the amine-protonated *para*-benzocaine deviates so much from the experiment.

After standard-level optimization, O_{CO} and N_{NH2} protomers of *ortho*-benzocaine have computed CCS values of 131.0 and 131.5 Å^2, respectively. Based on these values, assignment of the single experimentally observed peak to either protomer is difficult, as

they are expected to be almost indistinguishable. It is therefore impossible to say whether they both occur in the gas phase, with their peaks overlapping, or if only one of them is present. In this context it is worth noting that a recent report proposed the two alternative forms of deprotonated *ortho*-hydroxybenzoic acid to be connected by a relatively low isomerization barrier[29]. It might therefore be considered likely that the protomers of *ortho*-benzocaine could also easily convert due to intramolecular H-bonding, leading to only one mobility signal.

Two distinct CCS values are calculated after standard-level optimization for *meta*-benzocaine: 133.9 $Å^2$ for the O_{CO} isomer and 140.8 $Å^2$ for the N_{NH2} protomer. While such calculations predict reasonably well if the postulated protomers will be separated by ion mobility (one or two peaks expected), the absolute CCS values do not always match well with the measured ones, e.g. for the N_{NH2} form of *meta*-benzocaine.

The calculated CCS value of the N protomer of aniline (at "standard" level) is also not well matched with either of the experimental values (112.9 $Å^2$ and 118.0 $Å^2$). The ring-protonated species should be assigned to the first peak in the ATD, based on data reported in the literature[25].

3.5 Evaluating different levels of DFT calculations

Although the majority of ion mobility studies employ the commonly used B3LYP functional with 6-31G or 6-311G basis sets, a wide variety of other functionals and basis sets are available. Because the CCS values computed so far, using the "standard" level combined with the N_2-modified MobCal code, still show some discrepancies with the experiment, we also used B3PW91/def2-TVZP (hereafter called "high" level) in order to assess how sensitive the computed values are to the DFT parameters. Tables 1, 3 and 4 and Figures S.2 to S.9 contrast "standard" with high-level calculated CCS values.

For the benzocaine isomers and aniline, we found that the high-level calculations yield generally better matches against the experimental values (Table 1).

Both postulated protomers of DOH are found to have similar CCS at "high" level, which also closely match the single observed peak centred at 165.3 $Å^2$. The "standard" level result, where the CCS value for the N_{AA} protomer was underestimated (156.1 $Å^2$), falsely suggested that two distinct DOH protomers should exist, with a ΔCCS_{N2} of 8.5 $Å^2$ (Table 3).

For the $DOCH_3$ form of melphalan on the other hand, the CCS values calculated at both levels of structural optimization (around 180 $Å^2$) are significantly higher than the

measured one (172.2 $Å^2$). It is not apparent though why CCS calculations for this compound deviate so much from the experiment.

For melphalan itself, the expected improvement in the theoretical values is also less pronounced when using the B3PW91 functional and larger basis set. Notably the CCS of the N_{Cl} protomer is now overestimated: 170.6 $Å^2$ ("standard" level) vs. 174.1 A^2 ("high" level). Since the experimentally derived value for this protomer is 169.9 $Å^2$, the "standard" level result is in better agreement in this particular case. While the reason for this anomaly is not entirely clear, melphalan stands out as a compound with the highest conformational "flexibility" (see below) in the group studied here.

We show here that for a number of structurally related compounds, the calculation of "best" molecular geometries and charge distributions using two different levels of DFT calculations leads to mixed results, with respect to how well the derived CCS match with experimentally observed CCS (see Figure 5). Contrary to what we might have expected, the high-level calculations do not always agree better with experiment. A more thorough investigation of different basis sets and functionals is needed, as well as a re-parametrization of CCS calculation methods, which currently rely on modifications to the existing MobCal code. Such efforts are now underway in different research groups.

3.6 Effect of charge distribution on CCS calculations

Although this study assumes that different protonation site isomers can be formed in the electrospray process and observed via their characteristic mobility peaks, the question still remains to what extent different factors contribute to protomer separation in ion mobility: is it the charge site itself, or rather the conformational change driven by alternative charge sites? As an example of the latter, the rotation of the chloroethyl groups in the mustard moiety of melphalan could lead to the observation of multiple conformers. Interaction of these chloroethyl groups with the phenylalanine moiety of the molecule could possibly also result in more compact ions.

Protonation at different sites, which results in different charge distributions (after optimization) across the molecule, can potentially affect its geometry (i.e. the atomic positions) in a way that contributes to a change in CCS. In order to assess the magnitude of this effect separately from that of the charge distribution itself, we simply recalculated the CCS, while removing the atomic partial charges. These re-calculated CCS values are reported in Table 5 ("no charge distribution"). Removing the charges drastically lowers the computed CCS values, as expected in N_2 drift gas particularly for the smaller analytes

(benzocaine isomers and aniline), and we do not expect them to match the experimental values anymore. More importantly, what this exercise can show is if the calculated CCS difference between two postulated protomers is maintained even in the absence of any charge, i.e. whether it is largely caused by a conformational change of the molecule. This is the case only for the melphalan protomers. All other molecules studied here show virtually identical CCS (within the error margin of the experiment) for the "uncharged" protomer pairs. This signifies that the potentially different molecular geometries of the protomers, optimised in the presence of charge, would not account for any possible CCS difference. Rather the position of the proton and the resulting relatively large differences in charge distributions and dipole moments are held responsible for the observed protomer separation in ion mobility. We can speculate that of the molecules studied here, only melphalan is "flexible" enough to undergo a charge-site driven conformational change which is sufficiently large to contribute to the separation of its protomer peaks. These calculations show that different protonation sites can yield significantly different ion mobilities in nitrogen, indicating that the long-range electrostatic contribution of the charge to the overall CCS is substantial.

3.7 Protomers and dipole moments

The analysis of the effect of molecular geometry on CCS independent of charge (see section 3.6) showed that for some of the small molecules studied here, charge distributions are the determining factor for their separation in ion mobility when using polarizable gases. A close look at the structures of the protomer pairs shows that, although their mobilities can differ considerably, their geometries may indeed be relatively similar. Since the atomic coordinates of these structures only vary slightly (apart from melphalan), the CCS difference is thought to be predominantly the result of the charge distribution. The differences between the molecular dipole moment of various protomers could therefore be used as a possible predictor for the separation of these protomers in ion mobility[30].

As an example, the charge distributions of the three melphalan protomers considered here are visualized as molecular electrostatic potentials (MEPs) in Figure 4. Comparison of the 5 lowest-energy structures per protonation site (see Table 2) shows that they share similar dipole moments. Furthermore, the structures with the smallest dipole moment (ca. 6 Debye) also correspond to the ion with the smallest CCS value, i.e. the N_{Cl} protomer. The structures that have a dipole moment of around 11 Debye correspond to the ion with

the largest observed CCS value (N_{AA} protomer). We plotted all 4 experimentally observed protomer pairs with their ΔCCS values against the corresponding Delta dipole values, calculated at the best-fitting DFT level (apart from melphalan, all "high" level; see Figure 6). Although the correlation is not very strong, the trend is clear: the larger the calculated Delta dipole values, the higher the measured Delta CCS.

To test this hypothesis further, we also plotted predicted ΔCCS values for all possible protomer pairs, calculated at both "standard" and "high" levels using MobCal, against their corresponding Delta dipole values. These data highlight that the correlation between CCS and dipole moment is quite poor with standard-level calculations (red squares in Figure 6). The high-level structure calculations on the other hand (blue diamonds) yield a reasonably good correlation (linear fit: R^2=0.8784) between differences in dipole moment of protomer pairs and their separation in ion mobility experiments where polarisable drift gases such as nitrogen are used[30,31]. Aniline shows a ΔCCS larger than expected based on the calculated Δ dipole value, which may be due to the fact that the smaller protomer is a ring-protonated (charge-delocalized) form.

Taken together, these data suggest that rather than geometry or net charge alone, the charge distribution – characterized by the dipole moment and, as recently proposed[29], the polarizability of the analyte – plays a major role for the observed CCS values as well, particularly for relatively rigid molecules and their specific interaction with a polarizable drift gas (i.e. N_2). Experimentally observed protomer separation is found to be explained reasonably well by differences between the calculated dipole moments of alternatively protonated forms of the analyte.

4. Experimental

Caution: melphalan and degradation products are carcinogenic and should be handled with care.

4.1. Chemicals and sample preparation

Chemicals purchased from Sigma-Aldrich (Bornem, Belgium): acetaminophen (> 99.0 %), alprenolol (Eur. Pharmacop. Ref.), aniline (99.8 %), colchicine (> 95 %), dexamethasone (> 97 %), ethyl 4-aminobenzoate (98 %), ethyl 3-aminobenzoate (97 %),

ethyl 2-aminonenzoate (> 99 %), N-ethylaniline (98 %), melphalan (min. 95 %), ondansetron (> 98 %), poly-DL-alanine, sodium formate (HPLC, > 99.0 %) and verapamil (> 99 %). Acetonitrile (ACN; HPLC grade), methanol (MeOH; HPLC grade) and formic acid (FA; 99+ %) were obtained from Acros (Geel, Belgium). Reversed osmosis (RO) water was prepared using a Silex water filtering system from Eurowater (Nazareth-Eke, Belgium). Ammonium hydroxide (solution of 25 % v/v) was purchased from Merck (Overijse, Belgium). Dimethoxymelphalan was synthesized in-house, and dihydroxymelphalan formed during synthesis as an additional reaction product. Stock solutions (10^{-2} M) of all analytes and calibrants were prepared in MeOH.

4.2 Optimisation of molecular structures and charge distributions

A conformational analysis was performed to find the best structure of melphalan ions in the gas phase. The conformational space of the different protonated species ('protomers') was explored using TINKER (version 6)[45] with the Merck molecular force field (MMFF94). The resulting structures were further optimised with Gaussian 09[46] at the B3LYP/6-31G(d,p) ("standard") and B3PW91/def2-TZVP ("high") levels. For each calculation, the optimised structure was verified to be a local minimum by performing a vibrational analysis. Atomic charges were computed using the Merz-Singh-Kollman scheme with the constraint to reproduce the molecular dipole ('pop=mk,dipole'). The uncharged structures were generated by simply removing the atomic partial charges. As the dipole moment for charged species depends on the origin chosen, the center of charge was used as a reference point instead of the center of mass for all calculations. Three-dimensional structures were visualized using Avogadro (version 1.1.1)[47] and molecular electrostatic potentials (MEPs) using VMD (version 1.9.2)[48,49].

4.3 Calculation of CCS values

MobCal was used to calculate CCS values[32,33]. MobCal is available as freeware[50]. MobCalPARSER, also available as freeware[51], allowed the direct use of Gaussian output (.log) files.

The modified version of MobCal[41] used in this study calculates CCS values for experiments in nitrogen drift gas and takes into account ion-quadrupole interactions and the orientation of non-spherical gases during collisions (TM algorithm only). Lennard-Jones potentials were re-tuned by scaling universal force field (UFF) parameters such as the atomic energy and van-der-Waals distance, in order to represent the ion

motion through N_2 drift gas better. The code was also expanded with other types of atoms.

4.4 Instrumentation

Travelling-Wave Ion Mobility Spectrometry (TWIMS) experiments were performed on a Synapt G2 HDMS instrument, and data acquisition and processing were carried out using MassLynx (V 4.1).

The instrument (Waters Corporation, Wilmslow, UK) was equipped with a nano-electrospray source and used gold-coated glass capillary needles, which were fabricated in-house. In order to obtain clean spectra, the ions under investigation were *m/z* selected in all IM-MS experiments. Prior to the experiments, the instrument was calibrated in the *m/z* 50-600 mass range using sodium formate solution (positive ion mode). All prepared solutions were checked for the presence of impurities, which might overlap with the signal of the analyte.

Typical instrument parameters in time-of-flight mode are: sample and extraction cone voltage: 10 V and 3 V, trap bias: 2 V, trap cell gas flow: 2 mL/min, trap and transfer CE: 4 V and 0 V. Experimental CCS are determined after a single calibration of the TWIMS cell using both poly-DL-alanine (0.5 mg/mL in 1:1 H_2O:ACN) and a set of drug-like compounds (5 μM each in 1:1 H_2O:ACN) as reported before[12,39]. In ion mobility mode, drift times were determined for different IM wave velocities in order to eliminate energy-dependent phenomena, which could affect the ion mobility separation. Some parameters differ in ion mobility mode: trap bias: 40 V, IMS wave velocity: 600 m/s or, for melphalan and related compounds: 1000 m/s, IMS wave height: 40 V, He and IMS (nitrogen) gas flow: 180 mL/min and 90 mL/min.

5. Conclusions

Most small compounds show only one, unique drift time in ion mobility experiments, which allows the use of such data as additional identifiers for mass-spectrometry based molecular characterization, e.g. in metabolomics. There is now considerable interest in assembling databases which contain ion mobilities of compounds under standardized conditions, not dissimilar to retention times in chromatography.

Occasionally, small molecules exhibit multiple ion mobility drift times, due to the ability to form different protomers. Protomers are constitutional isomers, or more precisely, isomeric catiomers. They are molecular species which originate from the same chemical entity in solution, but where partial, intramolecular proton transfer during electrospray ionization causes the formation of charge isomers in the gas phase. This is often encountered for, but not limited to, small molecules containing an amino and a carbonyl or carboxyl moiety. Protonation at different sites may not only distort the molecular geometry, affecting the hard sphere cross-sections, but also lead to significantly different charge distributions. The latter can be represented by the dipole moment, which has a large effect on the ion's mobility when polarisable drift gases such as nitrogen are used.

In the most systematic analysis to date, we utilized a panel of 7 closely related small molecules, 4 of which are found to show two drift time signals, to better understand what determines protomer separation in ion mobility and evaluate computational approaches for their characterization. IM-MS of the chemotherapeutic agent melphalan revealed the presence of two mobility peaks, whereas molecules closely related to this compound (i.e. dihydroxy- and dimethoxymelphalan) only showed one protonated form. For comparison, aniline and three isomers of benzocaine were also included in this study.

By comparing experimental with calculated CCS values from molecular modelling, we could assign the protonation site and structure of the observed ions. More flexible structures with bulky side chains (e.g. $DOCH_3$) however appear to have their CCS overestimated with both types of calculations used. While results of what we call “high-level” calculations match experimental data much better for most molecules studied here, a more systematic investigation of functionals and basis sets is required to determine the most appropriate computational strategy for the optimization of structure and charge of protomers. With different protonation sites in these compounds available under electrospray conditions, a number of alternative charge distributions and molecular geometries have to be evaluated for how well they match the corresponding collision cross sections in the experiment. More straightforward and efficient calculation methods would make this step much faster and more accurate, and enable “high-throughput” approaches for ion mobility data processing such as would benefit, e,g., compound identification in complex samples.

The use of polarisable drift gases (e.g. N_2), which has become common due to the widespread use of travelling wave IM-MS, leads to a more frequent observation of

protomer phenomena, and puts the issue of their structual assignment into the spotlight. We found a good agreement between experimental and theoretical CCS data in this study when using a modified version of the trajectory method, optimised for use with nitrogen as drift gas. Our data show that the molecular dipole moment, rather than the hard sphere collision cross section, is a useful determinant for the ion mobility separation of protomers. Furthermore, a good correlation appears to exist between the different calculated dipole moments, and both experimental and theoretical CCS differences, in protomer pairs investigated here. As calculated dipole moments are readily available, they may be useful "predictors" of protomer separation in experiments which target rapid small molecule isomer separation and identification using ion mobility.

Acknowledgements

Financial support by the Hercules Foundation Flanders allowing the purchase of the Synapt instrument and the CalcUA/VSC supercomputing cluster is acknowledged. We thank Iain Campuzano (Amgen, Thousand Oaks, CA, USA) for providing us with the modified MobCal algorithm and helpful discussions, and wish to thank the reviewers for their constructive feedback.

References

1. K. Giles, S. D. Pringle, K. R. Worthington, D. Little, J. L. Wildgoose and R. H. Bateman, *Rapid Comm. Mass Spectrom.*, 2004, **18**, 2401-2414.
2. K. Thalassinos, S. E. Slade, K. R. Jennings, J. H. Scrivens, K. Giles, J. Wildgoose, J. Hoyes, R. H. Bateman and M. T. Bowers, *Int. J. Mass Spectrom.*, 2004, **236**, 55-63.
3. H. A. Sawyer, J. T. Marini, E. G. Stone, B. T. Ruotolo, K. J. Gillig and D. H. Russell, *J. Am. Soc. Mass Spectrom.*, 2005, **16**, 893-905.
4. S. D. Pringle, K. Giles, J. L. Wildgoose, J. P. Williams, S. E. Slade, K. Thalassinos, R. H. Bateman, M. T. Bowers and J. H. Scrivens, *Int. J. Mass Spectrom.*, 2007, **261**, 1-12.
5. C. A. Scarff, K. Thalassinos, G. R. Hilton and J. H. Scrivens, *Rapid Commun. Mass Spectrom.*, 2008, **22**, 3297-3304 .

6. D. P. Smith, T. W. Knapman, I. Campuzano, R. W. Malham, J. T. Berryman, S. E. Radford and A. E. Ashcroft, *Eur. J. Mass Spectrom.*, 2009, **15**, 113-130.
7. C. W. N. Damen, Chen, A. B. Chakraborty, M. van Oosterhout, J. R. Mazzeo, J. C. Gebler, J. H. M. Schellens, H. Rosing and J. H. Beijnen, *J. Am. Soc. Mass Spectrom.*, 2009, **20**, 2021-2033.
8. C. Atmanene, S. Petiot-Bécard, D. Zeyer, A. Van Dorsselaer, V. Vivat Hannah and S. Sanglier-Cianférani, *Anal. Chem.*, 2012, **84**, 4703-4710.
9. A. Konijnenberg, A. Butterer and F. Sobott, *BBA - Proteins and Proteomics*, 2013, **1834**, 1239-1256.
10. B. T. Ruotolo, J. L. P. Benesch, A. M. Sandercock, S.-J. Hyung and C. V. Robinson, *Nat. Protoc.*, 2008, **3**, 1139-1152.
11. C. Uetrecht, R. J. Rose, E. Van Duijn, K. Lorenzen, and Albert J. R. Heck, *Chem. Soc. Rev.*, 2010, **39**, 1633-1655.
12. M. F. Bush, I. D. G. Campuzano, and C. V. Robinson, *Anal. Chem.*, 2012, **84**, 7124-7130.
13. J. L. Benesch and B. T. Ruotolo, *Curr. Opin. Struct. Biol.*, 2011, **21**, 641-649.
14. J. Snijder, R. J. Rose, D. Veesler, J. E. Johnson and A. J. R. Heck, *Angew. Chem. Int. Ed.*, 2013, **52**, 4020-4023.
15. L. Han and B. T. Ruotolo, *Int. J. Ion Mobil. Spectrom.*, 2013, **16**, 41-50.
16. M. Benassi, Y. E. Corilo, D. Uria, R. Augusti and M. N. Eberlin, *J. Am. Soc. Mass Spectrom.*, 2009, **20**, 269-277.
17. J. P. Williams, T. Bugarcic, A. Habtemariam, K. Giles, I. Campuzano, P. M. Rodger and P. J. Sadler, *J. Am. Soc. Mass Spectrom.*, 2009, **20**, 1119-1122.
18. M. Zhu, B. Bendiak, B. Clowers and H. H. Hill, *Anal. Bioanal. Chem.*, 2009, **394**, 1853-1867.
19. G. J. Dear, J. Munoz-Muriedas, C. Beaumont, A. Roberts, J. Kirk, J. P. Williams and I. Campuzano, *Rapid Commun. Mass Spectrom.*, 2010, **24**, 3157-3162.
20. M. Fasciotti, A. F. Gomes, F. C. Gozzo, B. A. Iglesias, G. F. de Sá, R. J. Daroda, M. Toganoh, H. Furuta, K. Araki and M. N. Eberlin, *Org. Biomol. Chem.*, 2012, **10**, 8396-8402.
21. L. Ahonen, M. Fasciotti, G. B. A. Gennäs, T. Kotiaho, R. J. Daroda, R. M. Eberlin and R. Kostiainen, *J. Chromatogr. A*, 2013, **1310**, 133–137.
22. V. E. Wright, F. Castro-Gómez, E. Jurneczko, J. C. Reynolds, A. Poulton, S. D. R. Christie, P. Barran, C. Bo and C. S. Creaser, *Int. J. Ion Mobil. Spec.*, 2013, **16**, 61–67.
23. J. P. Williams, J. M. Brown, I. Campuzano and P. J. Sadler, *Chem. Commun.*, 2010, **46**, 5458-5460.
24. J. Hofmann, H. S. Hahm, P. H. Seeberger and K. Pagel, *Nature*, 2015, **526**, 241-244.

25. P. M. Lalli, B. A. Iglesias, H. E. Toma, G. F. Sa, R. J. Daroda, J. C. Silva Filho, J. E. Szulejko, K. Araki and M. N. Eberlin, *J. Mass Spectrom.*, 2012, **47**, 712-719.
26. A. Kaufmann, P. Butcher, K. Maden, M. Widmer, K. Giles and D. Uria, *Rapid Commun. Mass Spectrom.*, 2009, **23**, 985-998.
27. C. Lapthorn, T. J. Dines, B. Z. Chowdhry, G. L. Perkins and F. S. Pullen, *Rapid Commun. Mass Spectrom.*, 2013, **27**, 2399-2410.
28. S. Warnke, J. Seo, J. Boschmans, F. Sobott, J. H. Scrivens, C. Bleiholder, M. T. Bowers, S. Gewinner, W. Schöllkopf, K. Pagel and G. von Helden, *J. Am. Chem. Soc.*, 2015, **137**, 4236-4242.
29. R. S. Galaverna, G. A. Bataglion, G. Heerdt, G. F. de Sa, R. Daroda, V. S. Cunha, N. H. Morgon, M. N. Eberlin, Eur. *J. Org. Chem.*, 2015, **2015**, 2189-2196.
30. P. M. Lalli, Y. E. Corilo, M. Fasciotti, M. F. Riccio, G. F. de Sá, R. J. Daroda, G. H. M. F. Souza, M. McCullagh, M. D. Bartberger, M. N. Eberlin and I. D. G. Campuzano, *J. Mass Spectrom.*, 2013, **48**, 989-997.
31. T. G. Flick, I. D. G. Campuzano and M. D. Bartberger, *Anal. Chem.*, 2015, **87**, 3300-3307.
32. M. F. Mesleh, J. M. Hunter, A. A. Shvartsburg, G. C. Schatz, and M. F. Jarrold, *J. Phys. Chem.*, 1996, **100**, 16082-16086.
33. A. A. Shvartsburg and M. F. Jarrold, *Chem. Phys. Lett.*, 1996, **261**, 86-91.
34. T. W. Knapman, J. T. Berryman, I. Campuzano, S. A. Harris and A. E. Ashcroft, *Int. J. Mass Spectrom.*, 2010, **298**, 17-23.
35. C. Bleiholder, T. Wyttenbach and M. T. Bowers, *Int. J. Mass Spectrom.*, 2011, **308**, 1-10.
36. S. E. Anderson, C. Bleiholder, E. R. Brocker, P. J. Stang and M. T. Bowers, *Int. J. Mass Spectrom.*, 2012, **330-332**, 78-84.
37. C. Bleiholder, S. Contreras, T. D. Do and M. T. Bowers, *Int. J. Mass Spectrom.*, 2013, **345-347**, 89-96.
38. C. Bleiholder, S. Contreras and M. T. Bowers, *Int. J. Mass Spectrom.*, 2013, **354-355**, 275-280.
39. E. G. Marklund, M. T. Degiacomi, C. V. Robinson, A. J. Baldwin and Justin L.P. Benesch, Collision Cross Sections for Structural Proteomics, *Structure*, http://impact.chem.ox.ac.uk, (accessed May 2015).
40. D. Guillarme, H. Kim, J. Ruta, H. I. Kim, S. Rudaz, P. V. Johnson, J.-L. Veuthey, L. W. Beegle, J. L. Beauchamp, W. A. Goddard and I. Kanik, *Anal. Chem.*, 2008, **80**, 1928-1936.
41. I. Campuzano, M. F. Bush, C. V. Robinson, C. Beaumont, K. Richardson, H. Kim, and H. I. Kim, *Anal. Chem.*, 2012, **84**, 1026–1033.
42. C. Lapthorn, F. S. Pullen, B. Z. Chowdhry, P. Wright, G. L. Perkins, and Y. Heredia,

Analyst, 2015, **140**, 6814-6823.

43. H. Lavanant, V. Tognetti and C. Afonso, *J. Am. Soc. Mass Spectrom.*, 2014, **25**, 572-580.
44. S. A. Stout and C. M. Riley, *Int. J. Pharm.*, 1985, **24**, 193-208.
45. TINKER – Software Tools for Molecular Design, http://dasher.wustl.edu/tinker, (accessed January 2015).
46. M. J. Frisch, G. W. Trucks, H. B. Schlegel, G. E. Scuseria, M. A. Robb, J. R. Cheeseman, G. Scalmani, V. Barone, B. Mennucci, G. A. Petersson, H. Nakatsuji, M. Caricato, X. Li, H. P. Hratchian, A. F. Izmaylov, J. Bloino, G. Zheng, J. L. Sonnenberg, M. Hada, M. Ehara, K. Toyota, R. Fukuda, J. Hasegawa, M. Ishida, T. Nakajima, Y. Honda, O. Kitao, H. Nakai, T. Vreven, J. A. Montgomery, Jr., J. E. Peralta, F. Ogliaro, M. Bearpark, J. J. Heyd, E. Brothers, K. N. Kudin, V. N. Staroverov, R. Kobayashi, J. Normand, K. Raghavachari, A. Rendell, J. C. Burant, S. S. Iyengar, J. Tomasi, M. Cossi, N. Rega, J. M. Millam, M. Klene, J. E. Knox, J. B. Cross, V. Bakken, C. Adamo, J. Jaramillo, R. Gomperts, R. E. Stratmann, O. Yazyev, A. J. Austin, R. Cammi, C. Pomelli, J. W. Ochterski, R. L. Martin, K. Morokuma, V. G. Zakrzewski, G. A. Voth, P. Salvador, J. J. Dannenberg, S. Dapprich, A. D. Daniels, Ö. Farkas, J. B. Foresman, J. V. Ortiz, J. Cioslowski, D. J. Fox, Gaussian 09, Revision D.01, Gaussian, Inc., Wallingford CT, 2009.
47. Avogadro – An Open-source Molecular Builder and Visualization Tool, http://avogadro.cc/wiki/Main_Page, (accessed May 2015).
48. VMD – Visual Molecular Dynamics, http://www.ks.uiuc.edu/Research/vmd, (accessed January 2015).
49. W. Humphrey, A. Dalke and K. Schulten, VMD - Visual Molecular Dynamics, *J. Molec. Graphics*, 1996, **14**, 33-38.
50. MobCal – A Program to Calculate Mobilities, http://www.indiana.edu/~nano/software.html, (accessed May 2015).
51. MobCalPARSER, http://sourceforge.net/projects/mobcalparser, (accessed May 2015).
52. Collision Cross Section Database, http://depts.washington.edu/bushlab/ccsdatabase, (accessed February 2015).

Figures

Graphical abstract

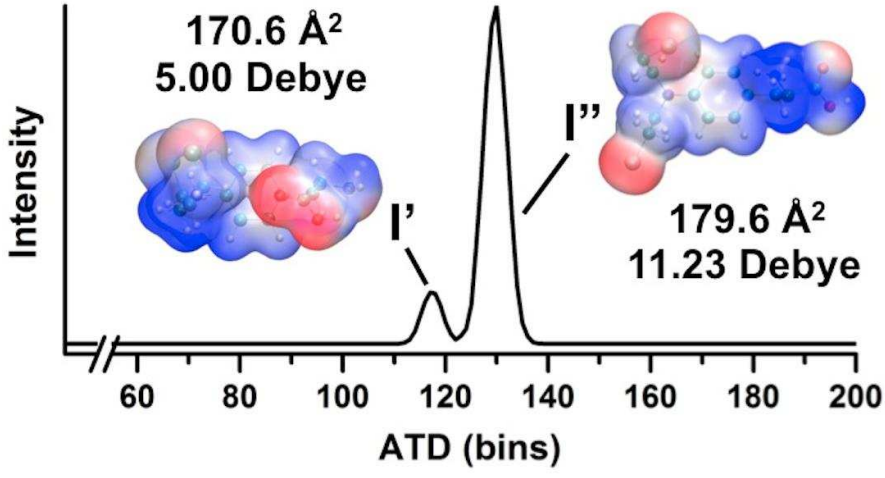

582 Figure 1

583 Overview of the sequence and output of the various experiments and calculations.

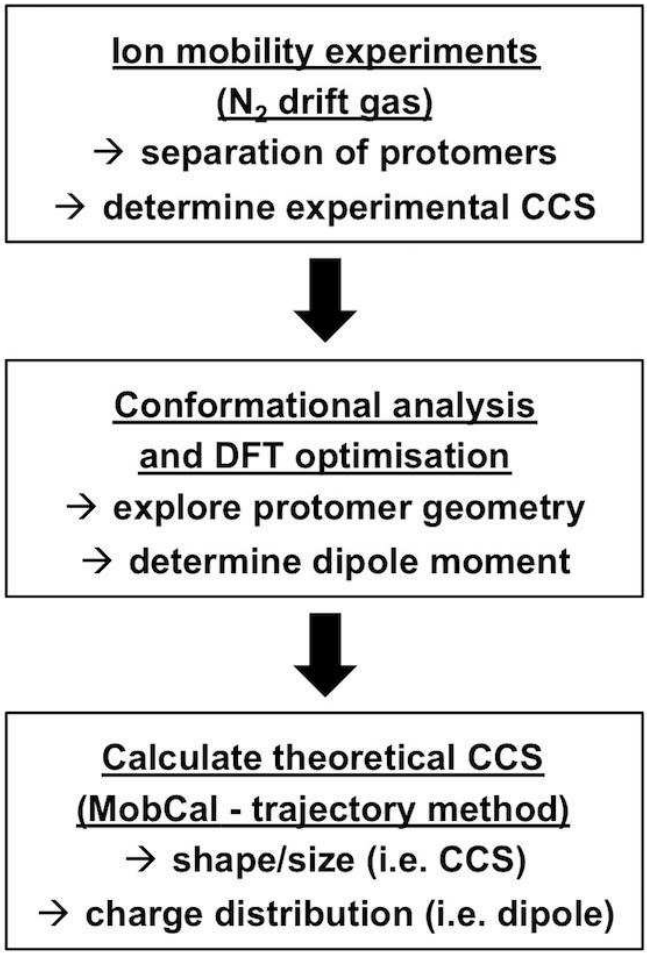

584

585 Figure 2:

586 Observation of two peaks for melphalan (**I**; top panel), but only one peak for the $DOCH_3$

587 (**II**) and DOH (**III**) hydrolysis products. The drift time difference between the two

588 melphalan peaks is larger than the difference between DOH and $DOCH_3$.

589

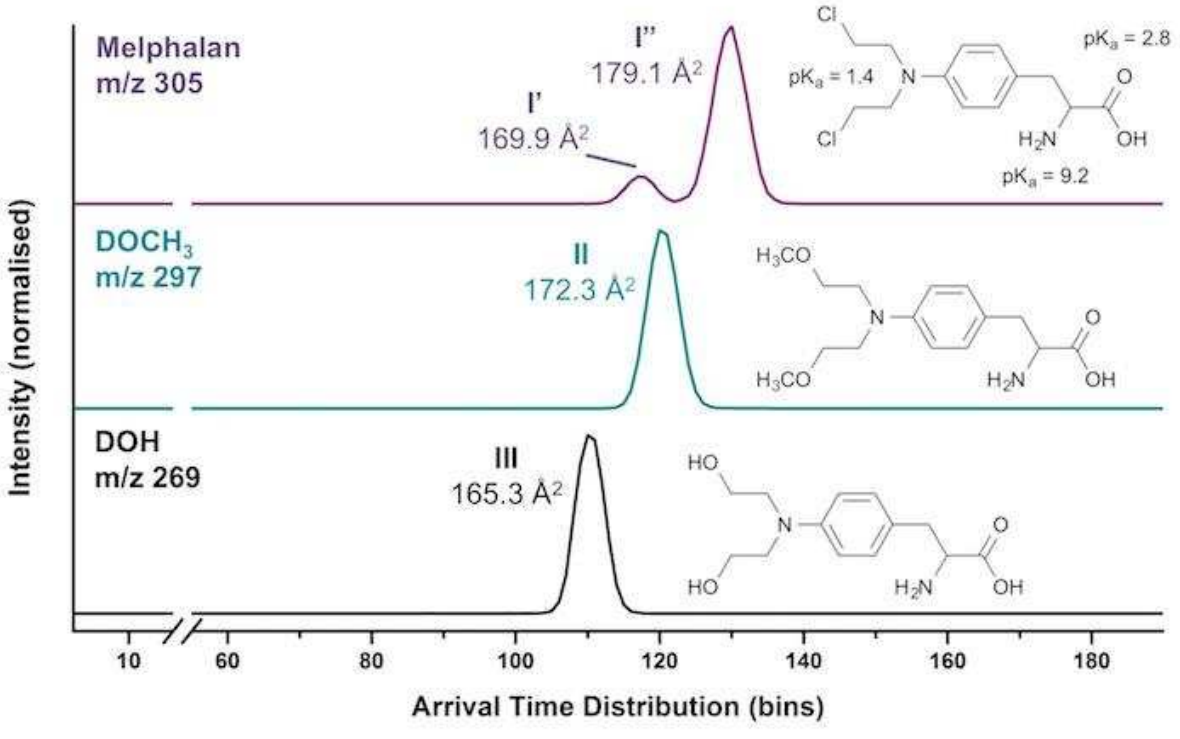

590

591

592

Figure 3:

Observation of two peaks for *para*-benzocaine (**IV**) and *meta*-benzocaine (**VI**) as well as aniline (**VII**). Only one peak is observed for *ortho*-benzocaine (**V**).

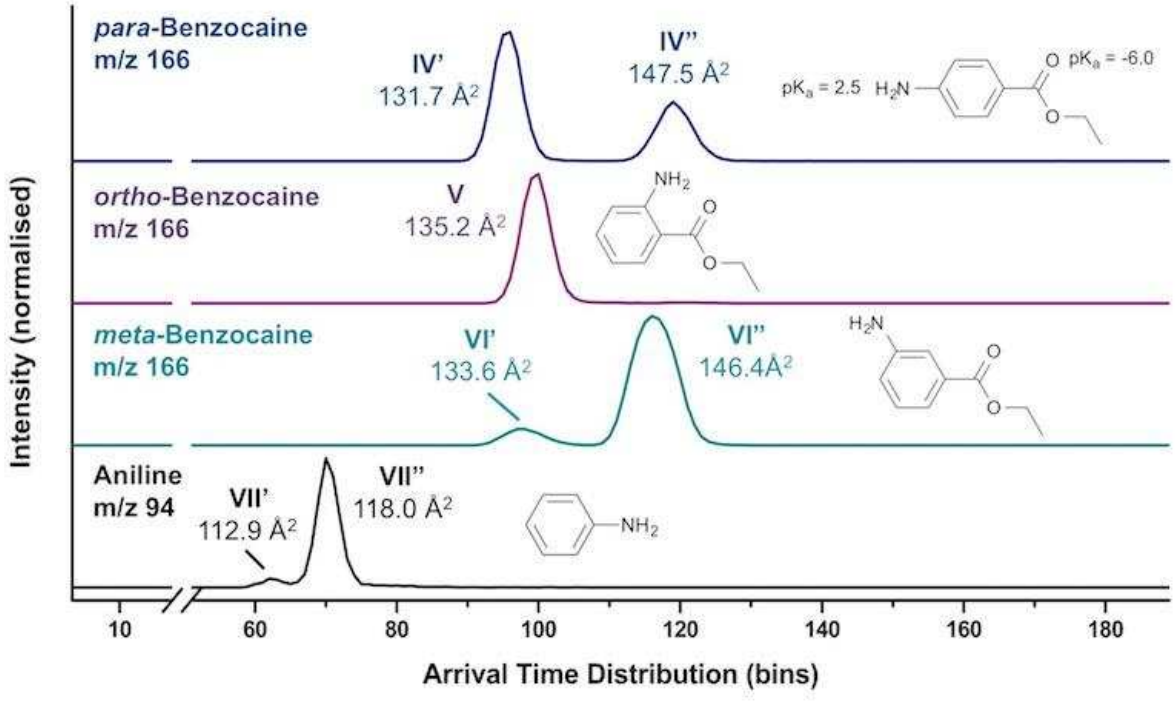

Figure 4

3D-visualisation of the lowest-energy structures of melphalan (**I**) after conformational analysis of the protonated molecules and subsequent standard-level DFT optimisation. Three possible protomers are shown: O_{CO} (left), N_{AA} (center) and N_{Cl} (right). Molecular electrostatic potentials (MEPs) are also given. Red areas display negative sites (e.g. electron dense) and blue areas more positive sites (e.g. protonated).

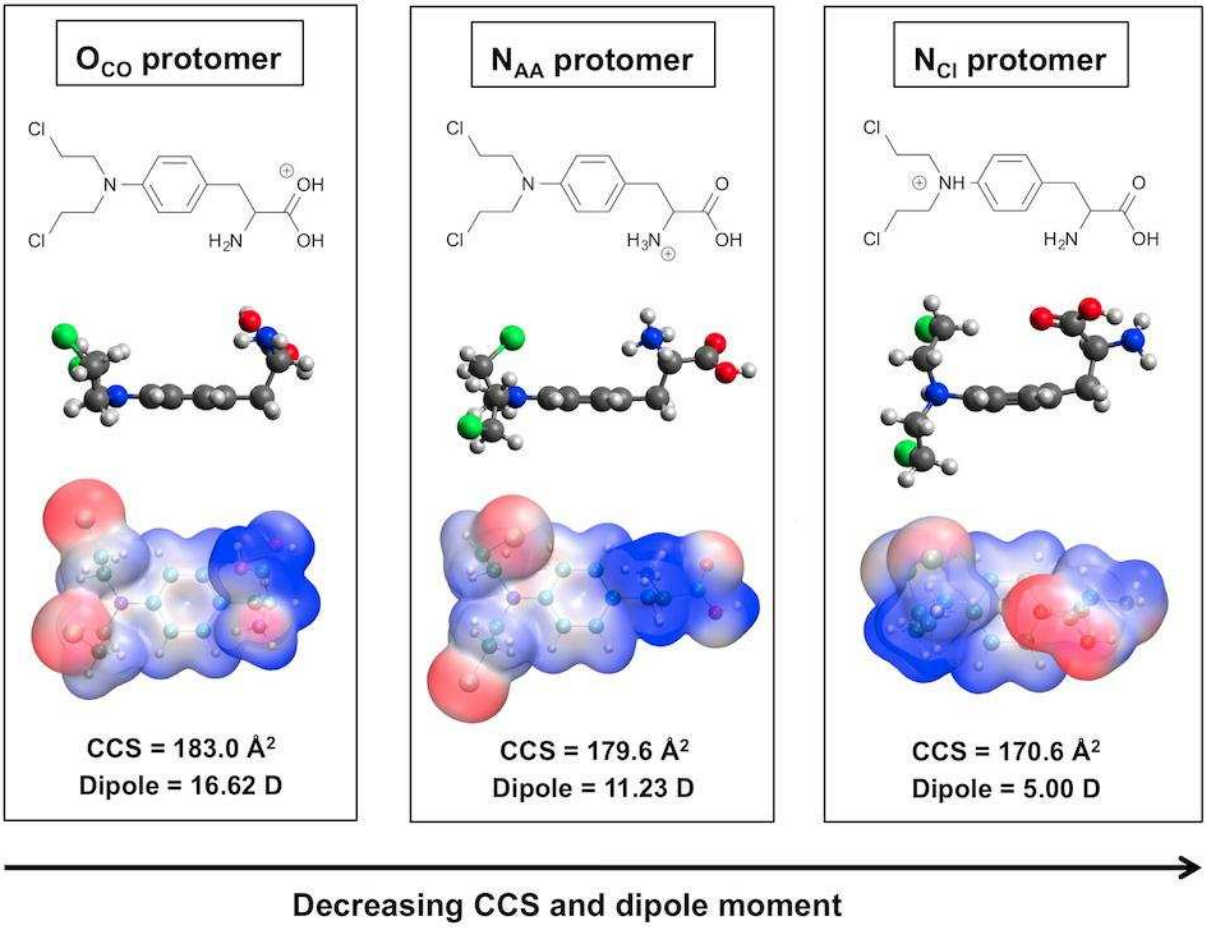

Figure 5

Visualisation of the experimental and calculated (both “standard” and “high” level) CCS values (Å^2) from Table 2 and 3. Only 4 of the 7 compounds investigated (**I**, **IV**, **VI**, and **VII**) are separated experimentally into protomer pairs (**I’/I’’** etc.), while for all of them CCS values were calculated for the 2 most plausible isoforms.

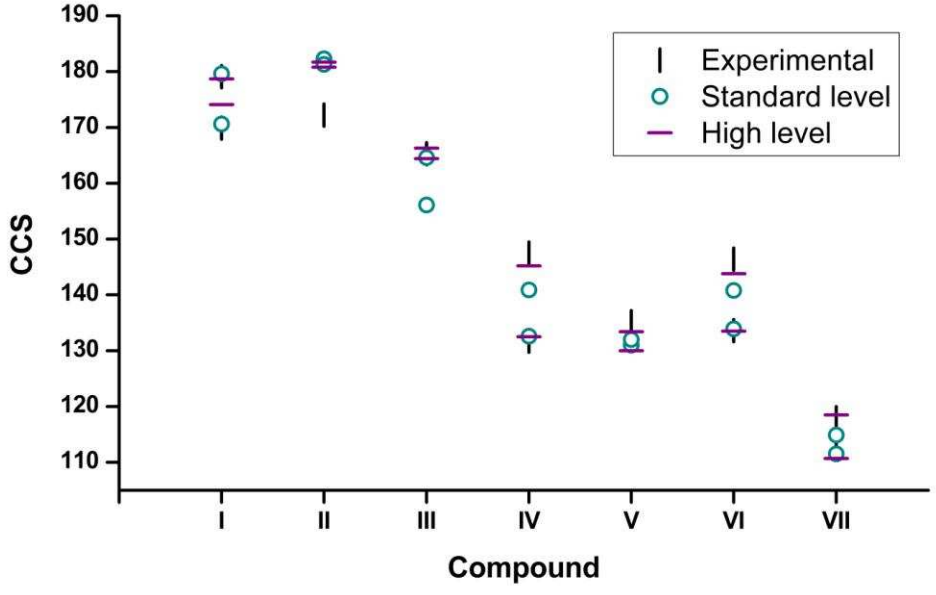

Figure 6

Correlation between calculated ΔCCS (Å^2) and Δ dipole moment (D) values for protomer pairs, using “standard” and high-level DFT calculations and the nitrogen-based MobCal software. For the 4 experimentally observed protomer pairs, the dipole moments were calculated using the best-fitting DFT level (apart from melphalan, all “high” level). At “high” level a linear fit (R^2=0.8784) suggests itself with aniline as an outlier, while at “standard” level, many calculated (Δ)CCS deviate from the experiment and no correlation is found with the calculated dipoles (R^2=0.1543).

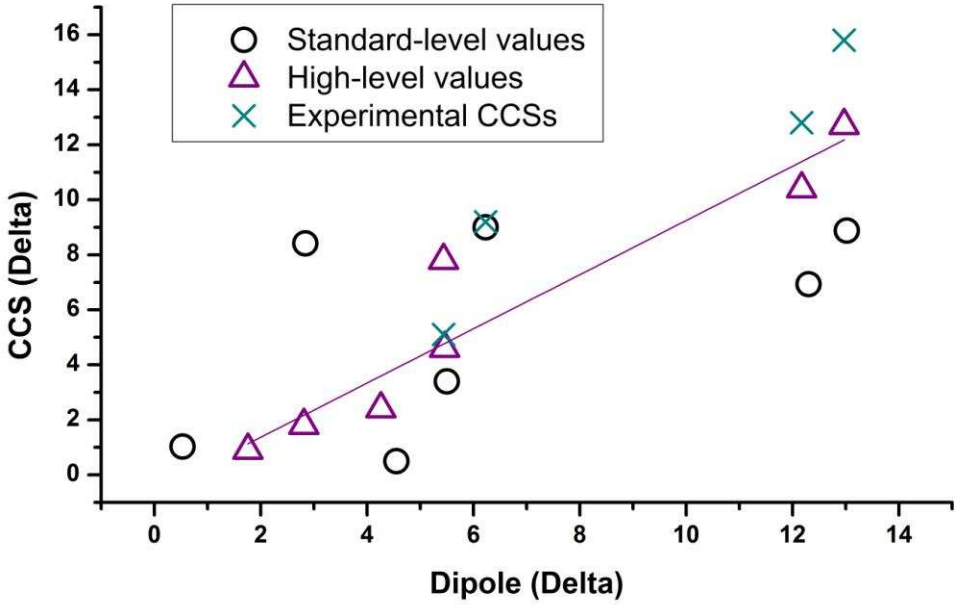

626 **Tables**

627

628 Table 1

629 Experimental CCS_{N2} values derived from TWIMS. MobCal-calculated CCS_{N2} using both
630 "standard" and high-level DFT optimizations are given for comparison. A detailed
631 overview of the calculated values can be found in Tables 2 and 3, together with calculated
632 energies, Boltzmann weights and dipole moments.

Analyte	Observed signal(s)	Protonation site	$CCS_{exp.}$ (Å^2) (Synapt G2 HDMS)	$CCS_{calc.}$ (Å^2) Standard level	$CCS_{calc.}$ (Å^2) High level
Melphalan (Mel)	**I'**	N_{Cl}	169.9 (± 1.5)	170.6	174.1
	I"	N_{AA}	179.1 (± 0.9)	179.6	178.7
Dimethoxymelphalan ($DOCH_3$)	**II**	N_{OCH3}	172.2 (± 0.9)	182.3	181.7
		N_{AA}		181.3	180.8
Dihydroxymelphalan (DOH)	**III**	N_{OH}	165.3 (± 0.6)	164.6	166.3
		N_{AA}		156.1	164.4
para-benzocaine	**IV'**	O_{CO}	131.7 (± 0.8)	132.6	132.5
	IV"	N_{NH2}	147.5 (± 0.6)	140.9	145.2
ortho-benzocaine	**V**	O_{CO}	135.2 (± 0.3)	131.0	131.0
		N_{NH2}		132.0	133.4
meta-benzocaine	**VI'**	O_{CO}	133.6 (± 1.1)	133.9	133.5
	VI"	N_{NH2}	146.4 (± 0.8)	140.8	143.8
Aniline	**VII'**	ring (*para*-)	112.9 (± N/A)	111.5	110.7
	VII"	N_{NH2}	118.0 (± 2.8)	114.9	118.5

Underlined values represent best matching calculated and experimental CCS values

633

634

635 Table 2

636 Overview of the 5 lowest-energy melphalan structures for each protomer. Structures were
637 acquired after conformational analysis of the protonated molecule, followed by
638 standard-level DFT optimization. The global E ranking and energies (relative to the
639 lowest-energy structure) give an indication of which protonation sites are most favored in
640 the gas-phase. Note the significantly different dipole moments for the N_{AA}/O_{CO} and N_{Cl}
641 structures.

Protonation site	E-ranking (relative)	E-ranking (global)	Rel. E (kcal/mol)	Boltzmann weight (%)	Dipole (Debye)	$CCS_{calc.}$ ($Å^2$)
N_{AA}†*	1	1	0.0000	10.87	11.23	179.6
	2	2	0.0220	10.47	11.49	177.3
	3	3	0.0878	9.37	11.38	181.0
	4	4	0.1908	7.87	12.66	179.2
	5	5	0.1995	7.76	12.26	176.6
N_{Cl}	1	17	1.0718	1.78	5.00	170.6
	2	23	1.2669	1.28	7.55	170.5
	3	30	2.6268	0.13	7.72	170.1
	4	33	3.1156	0.06	4.77	172.4
	5	37	3.6565	0.02	4.70	177.5
O_{CO}	1	151	31.0944	0.00	16.62	183.0
	2	152	34.4133	0.00	18.33	182.3
	3	153	34.4195	0.00	18.13	185.6
	4	154	35.4411	0.00	22.65	184.1
	5	155	37.1824	0.00	16.86	181.2

Underlined values represent calculated CCS values for lowest-energy structures
† Expected protonation site in solution (i.e. based on pK_a)
* Favoured protonation site in the gas phase (i.e. based on Boltzmann weights)

642

643

Table 3

Overview of the lowest-energy structure for each protomer of dimethoxy- and dihydroxymelphalan ($DOCH_3$ and DOH). Structures were acquired after conformational analysis of the protonated molecule and both "standard" and high-level DFT optimization. Note that, unlike melphalan, N_{AA} is the least favored protomer. Similar dipole moments are observed for each protonation site. The global energy ranking is given for each compound and per DFT optimization level.

Analyte	Protonation site	DFT opt. level	E-ranking (per level)	Relative E (kcal/mol)	Boltzmann weight (%)	Dipole (Debye)	$CCS_{TM,N2}$ ($Å^2$)	$CCS_{exp.}$ ($Å^2$)
Mel (**I**)	N_{AA}†*	Standard	1	0.0000	10.87	11.23	179.6	179.1 (± 0.9)
		High	1	0.0000	8.23	10.55	178.7	
	N_{Cl}	Standard	17	1.0718	1.78	5.00	170.6	169.9 (± 1.5)
		High	5	0.2027	5.85	5.09	174.1	
$DOCH_3$ (**II**)	N_{AA}†	Standard	126	7.5470	0.00	8.50	181.3	172.2 (± 0.9)
		High	119	5.7718	0.01	9.78	180.8	
	N_{OCH3}*	Standard	1	0.0000	15.76	7.97	182.3	
		High	1	0.0000	11.98	8.02	181.7	
DOH (**III**)	N_{AA}†	Standard	26	4.7214	0.01	3.73	156.1	165.3 (± 0.6)
		High	34	5.3294	0.01	9.80	166.3	
	N_{OH}*	Standard	1	0.0000	35.99	6.57	164.6	
		High	1	0.0000	36.68	6.99	164.4	

† Expected protonation site in solution (i.e. based on pK_a)
* Favoured protonation site in the gas phase (i.e. based on Boltzmann weights)

Table 4

Overview of the lowest-energy structure for each of the benzocaine and aniline protomers, after conformational analysis of the protonated molecule and both "standard" and high-level DFT optimization. For all molecules (apart from *ortho*-benzocaine) significantly different CCS values are observed for both protomers. Standard-level DFT optimization tends to underestimate CCS values, but similar dipole moments are observed at both levels anyway.

Analyte	Protonation site	DFT opt. level	E-ranking (per level)	Relative E (kcal/mol)	Boltzmann weight (%)	Dipole (Debye)	$CCS_{TM,N2}$ (Å^2)	$CCS_{exp.}$ (Å^2)
para-benzocaine (**IV**)	O_{CO}*	Standard	1	0.0000	67.22	2.73	132.0	131.7 (± 0.8)
		High	1	0.0000	74.22	2.62	132.5	
	N_{NH2}†	Standard	5	11.6453	0.00	15.75	140.9	147.5 (± 0.6)
		High	5	11.9007	0.00	15.59	145.2	
ortho-benzocaine (**V**)	O_{CO}	Standard	5	9.9485	0.00	0.99	131.0	135.2 (± 0.3)
		High	3	9.9485	0.00	1.04	131.0	
	N_{NH2}†*	Standard	1	0.0000	68.58	5.54	131.5	
		High	1	0.0000	74.59	5.30	133.4	
meta-benzocaine (**VI**)	O_{CO}*	Standard	1	0.0000	45.62	0.96	133.9	133.6 (± 1.1)
		High	1	0.0000	57.02	0.87	133.5	
	N_{NH2}†	Standard	5	1.3987	4.30	13.25	140.8	146.4 (± 0.8)
		High	5	2.4900	0.85	13.05	143.8	
Aniline (**VII**)	ring (*para*-)*	Standard	1	0.0000	99.22	1.67	111.5	112.9 (± N/A)
		High	1	0.0000	90.60	1.62	110.7	
	N_{NH2}†	Standard	2	2.9687	0.68	7.18	114.9	118.0 (± 2.8)
		High	2	1.3535	9.36	7.07	118.5	

† Expected protonation site in solution (i.e. based on pK_a)

* Favoured protonation site in the gas phase (i.e. based on Boltzmann weights)

Table 5

Comparison of CCS values calculated for structures with or without their charge distribution. Apart from melphalan (**I**), the effect of the charge distribution is essential in order to calculate a distinct CCS for each of the compound's protomers.

Analyte	**Protonation site**	**$CCS_{calc.}$ ($Å^2$)**	
		Charge distr.	**No charge distr.**
Mel	N_{Cl}	170.6	149.0
(**I**)	N_{AA}	179.6	155.9
$DOCH_3$	N_{OCH3}	181.7	161.8
(**II**)	N_{AA}	180.8	161.5
DOH	N_{OH}	166.3	144.4
(**III**)	N_{AA}	164.4	142.0
para-benzocaine	O_{CO}	132.5	109.2
(**IV**)	N_{NH2}	145.2	109.4
ortho-benzocaine	O_{CO}	131.0	105.2
(**V**)	N_{NH2}	133.4	106.1
meta-benzocaine	O_{CO}	133.5	109.4
(**VI**)	N_{NH2}	143.8	108.8
Aniline	ring (*para*-)	110.7	76.6
(**VII**)	N_{NH2}	118.5	76.6